

Synthesis and Characterization of Novel Al-Matrix Composites Reinforced with Ti_3SiC_2 Particulates

S. Gupta, T. Hammann, R. Johnson, and M.F. Riyad

(Submitted September 18, 2014; in revised form November 10, 2014; published online December 4, 2014)

In this paper, we report for the first time, the synthesis and characterization of novel Ti_3SiC_2 reinforced Al-matrix composites. All the composites were cold pressed and sintered in the temperature range of 700–750 °C for 5–30 min in an inert Ar atmosphere. Microstructure analysis by scanning electron microscopy and phase analysis by x-ray diffraction confirmed that there was minimal interfacial reaction between Ti_3SiC_2 particles and Al. The addition of Ti_3SiC_2 enhanced the mechanical performance of the composites. For example, the pure Al samples had a yield strength of 97 ± 6 MPa, where as the volume fraction of Ti_3SiC_2 was increased to 5 and 10 vol.% in the composites, the yield strength increased significantly to 212 ± 27 and 273 ± 52 MPa, respectively. As the volume fraction of Ti_3SiC_2 was further increased to 20 and 35 vol.%, the yield strength mildly increased to 278 ± 48 MPa, and then decreased to 134 ± 20 MPa, respectively. The decrease in yield strength after 35 vol.% Ti_3SiC_2 addition in the Al matrix was attributed to the presence of higher amount of porosity in these samples. The addition of Ti_3SiC_2 particles also had a beneficial effect on the tribological performance of these composites against alumina substrates.

Keywords aluminum, composites, metallic matrix, powder metallurgy

1. Introduction

The $M_{n+1}AX_n$ (MAX) phases (over 60+ phases) are thermodynamically stable nanolaminates displaying unusual, and sometimes unique, properties (Ref 1–14). These novel phases possess a $M_{n+1}AX_n$ chemistry, where n is 1, 2, or 3, M is an early transition metal element, A is an A-group element and X is C or N. MAX phases are layered hexagonal (space group D4 h-P63/mmc) with two formula units per cell. The MAX phases are highly damage tolerant, thermal shock resistant, creep resistant, lubricious, readily machinable, and with Vickers hardness values of 2–8 GPa, are anomalously soft for transition metal carbides and nitrides (Ref 1–7, 14). Some of them are also oxidation resistant (Ref 8, 10–13). Due to the above mentioned properties, there is a huge potential that MAX Phases can be used for different structural applications.

The composites of MAX phases with metals (MAXMET) are also important from both a fundamental and an applied perspective. Zhang et al. (Ref 15) had proposed $\text{Cu}/\text{Ti}_3\text{SiC}_2$ as a new electrofriction material. Gupta et al. (Ref 14, 16) developed composites of MAX phases with Ag. These composites showed solid lubrication over a wide range of temperatures. Anasori et al. (Ref 17) reported on composites with up to 80 vol.% Mg with MAX phases. These composites are readily machinable, relatively stiff, strong, and light, and exhibit ultrahigh damping. Wang et al. (Ref 18) fabricated Al-matrix material composites from pure Al and 40 vol.% Ti_3AlC_2

powders using hot isostatic pressing technique. The yield strength of a Ti_3AlC_2 /aluminum composite was found to be twice that of aluminum. Hu et al. (Ref 19) reported the specific strength of an aluminum alloy/ Ti_2AlC composite was 50% higher than that of the peak-aged aluminum alloy in interpenetrating 40 vol.%—aluminum alloy composite. Recently, Kothalkar et al. (Ref 20) reported higher damping up to a stress of 200 MPa, which is better than any of the MAXMET composites in NiTi (Shape Memory Alloy)— Ti_3SiC_2 (MAX Phase) composite. Thus, there is a huge potential that multifunctional materials can be developed by using MAX phases as a constituent in Metal Matrix Composites (MMCs) or Ceramic Matrix Composites (CMCs).

It is well known that Al and Al alloys have poor tribological behavior (Ref 21). Aluminum-based MMCs reinforced with rigid ceramic particulates have high specific strength and modulus, good wear resistance as well as ease of processing. They have become increasingly important for structural applications in aerospace, automotive, and other transport industries (Ref 22, 23). Due to the incorporation of the hard particles, the machining of MMCs is difficult, and complex tools are necessary to machine them (Ref 24–26). It is expected, the addition of MAX Phases will further enhance the mechanical behavior of MMCs, and machinability. The novel MMCs will also have multifunctional attributes, for example, enhanced damping machinability, hardness, and tribological behavior. For rapid usage and fabrication of Al-MAX composites novel manufacturing methods should be explored.

In this paper, we report for the first time, the manufacturing and characterization of novel Al-matrix composites reinforced with Ti_3SiC_2 particulates.

2. Experimental Details

Ti_3SiC_2 powder (-325 mesh, Kanthal, Hallstahammar, Sweden) and the tailored concentrations of Al Powder

S. Gupta, T. Hammann, R. Johnson, and M.F. Riyad, Department of Mechanical Engineering, University of North Dakota, Grand Forks, ND 58201. Contact e-mail: surojit.gupta@engr.und.edu.

(-325 mesh, Alfa Aesar, Ward Hill, MA) were dry ball milled (8000 M mixer Mill, SPEX SamplePrep, Metuchen, NJ) for 2 min. All the compositions were dry milled with polymethyl methacrylate (PMMA) balls. The mixed powders were then cold pressed in a ~ 12.7 mm die at a uniaxial compressive stress ~ 210 MPa. Novel Al-matrix composites were designed by adding 35 vol.% (Al(65)-Ti₃SiC₂(35)), 20 vol.% (Al(80)-Ti₃SiC₂(20)), 10 vol.% (Al(90)-Ti₃SiC₂(10)), 5 vol.% (Al(95)-Ti₃SiC₂(5)) Ti₃SiC₂ in Al matrix, respectively. For comparison, pure Al samples were also prepared under similar conditions.

Due to difficulty in manufacturing samples with higher Ti₃SiC₂ content, Al(65)-Ti₃SiC₂(35) samples were fabricated by heating the samples at 10 °C/min to 760 °C, and then isothermal holding at 760 °C for 30 min in a tube furnace in an Ar environment. All other compositions were manufactured by heating the samples at 10 °C/min to 700 °C, and then isothermal holding at 700 °C for 5 min. The composites were then machined into ~ 3 mm cubes for characterizing mechanical behavior. Compression testing was done in a Shimadzu AG-IS UTM (Shimadzu AG-IS UTM, Shimadzu Scientific Instruments Inc., Columbia, MD). For each composition, a set of 5 samples were tested at a deflection rate of 1 mm/min. Due to experimental limitations, authors could not accurately measure the actual strain of each sample, hence stress versus displacement plots are reported. In the text, for qualitative comparison, yield strength is defined as the critical stress at which the stress transitions from linear to non-linear regime in the stress versus displacement plot. The linear regime had a regression fitting of $R^2 > 0.95$. An average of 5 yield strength measurements for each sample is reported in the text. The samples for hardness testing were polished ($R_a < 1$ μ m) and then tested on a Vicker's Hardness Indentor (Mitutoyo HM-112, Mitutoyo Corporation, Aurora, IL). Vickers hardness was measured by loading the samples at 9.8 N for 15 s. An average of five readings for each composition is reported in the text.

For the tribology measurements, all the samples were cut into tabs of ~ 4 mm \times ~ 4 mm \times ~ 3 mm. The samples were then polished until ~ 1 μ m finishing. Inconel 718 (California Metals and Supply Inc., Santa Fe Springs, CA) and alumina substrates (AL-D-42-2, AdValue Technology, Tucson, AZ) were also polished until ~ 1 μ m finishing. By a surface profilometer (Surfcom 480A, Tokyo Seimitsu Co. Ltd., Japan), it was confirmed that all the samples had $R_a < 1$ μ m.

All the tribology studies were then performed by a tab-on-disk tribometer (CSM Instruments SA, Peseux, Switzerland) at different loads of 2 N (~ 0.12 MPa), 5 N (~ 0.31 MPa), and 10 N (~ 0.62 MPa) and track radiuses of ~ 18 , ~ 14 , and ~ 10 mm on alumina substrates, respectively. An average of 10 final data points of the friction coefficient (μ) was used to calculate steady state friction coefficient (μ_f). The mass of the samples and substrates were measured before and after the testing by a weighing scale (Model AL204, Mettler Toledo, Columbus OH). The specific wear rate (WR) was calculated by using the following equation:

$$WR = (m_i - m_f) / (\rho \cdot N \cdot d), \quad (\text{Eq 1})$$

where m_i , m_f , ρ , N , and d is the initial mass, mass after testing, density of the composite, applied load, and total distance traversed by the tab during the tribology testing, respectively.

Samples were coated with Au/Pd using a sputter coater (SCD 030, BAL-TEC RMC, Tucson, AZ), and then mounted on aluminum mounts. Secondary electron (SE) and Backscat-

tered Electrons (BSE) images were obtained by using a Scanning Electron Microscope (JEOL JSM-6490LV, JEOL USA, Inc., Peabody, MA). X-ray information was obtained via a Thermo NanoTrace Energy Dispersive x-ray (EDS) detector with NSS-300e acquisition engine. It is important to note at this juncture that the accuracy of measuring C is quite low in the EDS. It follows implicitly, and unless otherwise noted, the compositions listed could very well contain C. This is especially true of sub-stoichiometric oxides. In addition, the chemistry of a region that was deemed chemically uniform at the micron level as quantified by EDS—is designated with two asterisks, as *microconstituent*, to emphasize that these areas are not necessarily single phases. The presence of C in these tribofilms is shown by adding {C_x} in the composition (Ref 14). For observing the grains, each sample was etched with Kelly's Reagent for 15 s and then it was rinsed with water.

X-ray Diffraction (XRD) measurements were performed on an AXS D8 Discover Bruker x-ray Diffraction System, an x-ray diffractometer equipped with a two-dimensional Hi-Star area detector, video camera / laser alignment system, and a Cu x-ray radiation point source.

3. Results and Discussion

3.1 Microstructure and Phase Analysis

Figure 1 shows the XRD profile of all the Al-Ti₃SiC₂ composites. In the XRD profile of Al(65)-Ti₃SiC₂(35) sample—Ti₃SiC₂, Al phases, TiC and Al₃Ti phases were detected. All the other compositions showed significantly small or negligible amount of Al₃Ti and TiC phases which indicate that there was mild or negligible reaction in these compositions. As mentioned earlier, Al(65)-Ti₃SiC₂(35) composition was fabricated at 760 °C for 30 min, whereas all the other compositions were fabricated at 700 °C for 5 min. Thus, the higher temperature during processing is responsible for greater reaction in the Al(65)-Ti₃SiC₂(35). During the optimization studies, despite several attempts, Al(65)-Ti₃SiC₂(35) could not be sintered at lower temperatures. Thus, alternative methods of fabrication like Hot Pressing (HP), or Hot Isostatic Press (HIP) should be explored for fabricating Al-Ti₃SiC₂ with higher concentrations of Ti₃SiC₂ (> 35 vol.%).

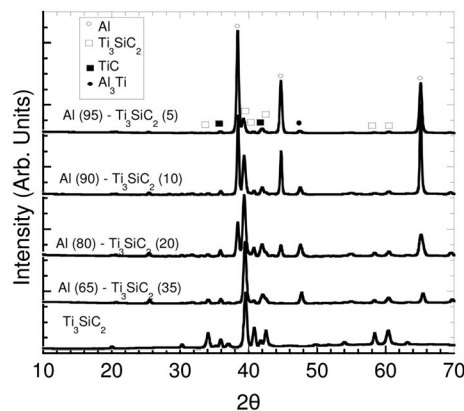


Fig. 1 XRD profiles of Al-Ti₃SiC₂ composites

Figure 2 shows the SE and BSE scanning electron microscopy (SEM) images of the etched surface of Al-MAX phase composites. In all the composites, Ti_3SiC_2 particles are well dispersed in the matrix. The grain size of all the compositions was similar and varied between 2–10 μm . Figure 3(a1) shows the SEM image of the polished surfaces of the Al(80)- Ti_3SiC_2 (20) composite. Figure 3(a2) and (a3) shows the SE and BSE image of a Ti_3SiC_2 particle embedded in it. No significant interfacial reaction was observed in the microstructure which further confirms XRD results.

3.2 Porosity and Mechanical Behavior

Figure 4(a) shows the change in porosity as a function of processing temperatures. The porosity changed linearly with the composition. This result shows that the processing of

Al-matrix composites by pressureless sintering becomes difficult as the concentration of Ti_3SiC_2 in the Al matrix increases. Figure 4(b) shows the compressive stress versus displacement profiles of all the Al-matrix composites. All the compositions, except Al(65)- Ti_3SiC_2 (35), showed gradual failure. The Al(65)- Ti_3SiC_2 (35) composition showed brittle failure. Figure 4(c) shows the comparison of yield strength and hardness for these composites. The Al had a yield strength of 97 ± 6 MPa, where as the volume fraction of Ti_3SiC_2 additions was increased to 5 and 10 vol.% in the composites, the yield strength increased significantly to 212 ± 27 and 273 ± 52 MPa, respectively. As the volume fraction of Ti_3SiC_2 was further increased to 20 vol.%, the yield strength mildly increased to 278 ± 48 MPa. However, in Al(65)- Ti_3SiC_2 (35), the yield strength decreased sharply to 134 ± 20 MPa. The hardness of the samples increased linearly as a function of Ti_3SiC_2 content.

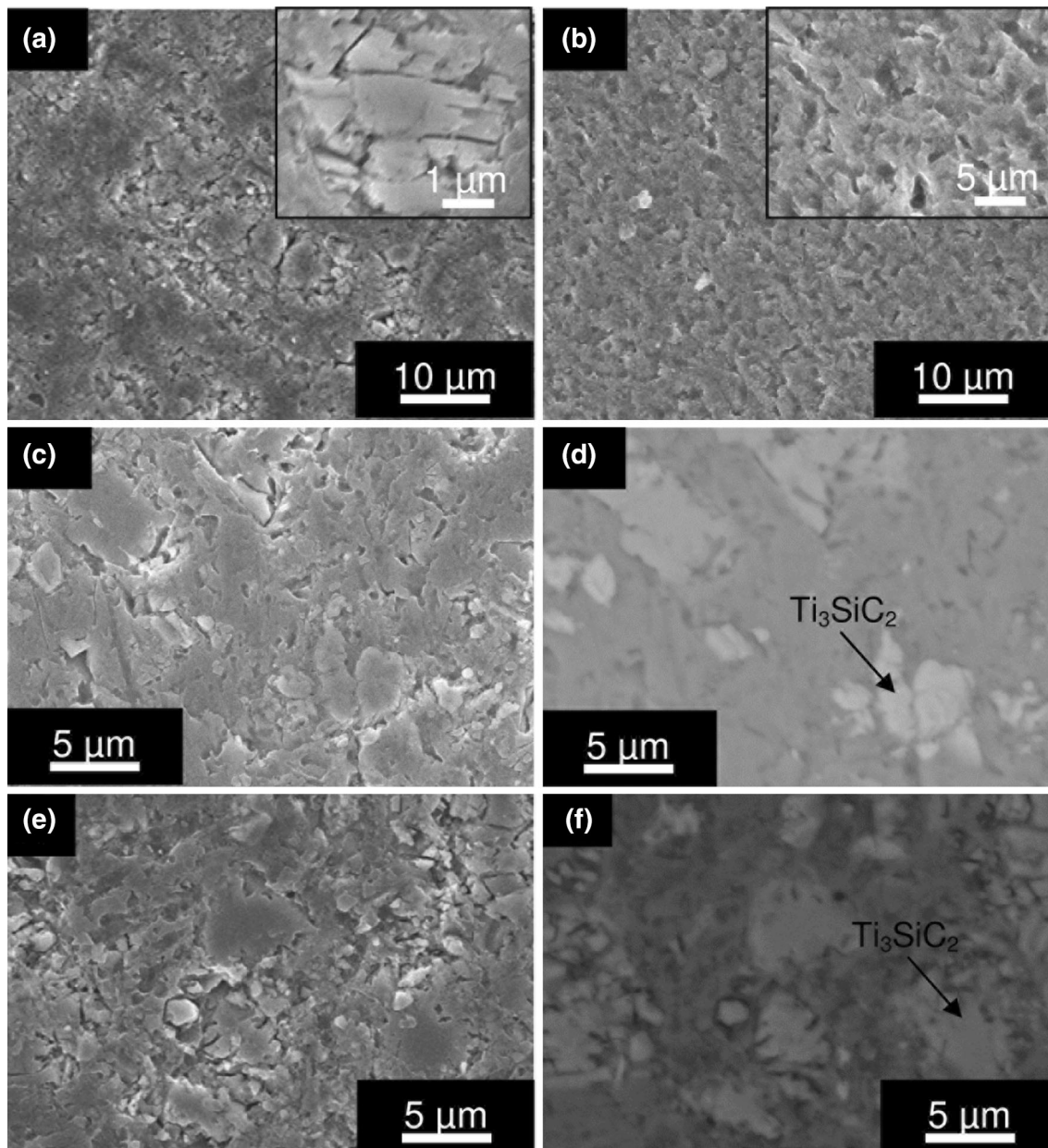


Fig. 2 SE SEM micrographs of etched surfaces of sintered, (a) Al (inset shows the grain structure), (b) Al(95)- Ti_3SiC_2 (5) (inset shows the grain structure), (c) Al(90)- Ti_3SiC_2 (10) and (d) BSE image of the same region, (e) Al(80)- Ti_3SiC_2 (20), and (f) BSE image of the same region

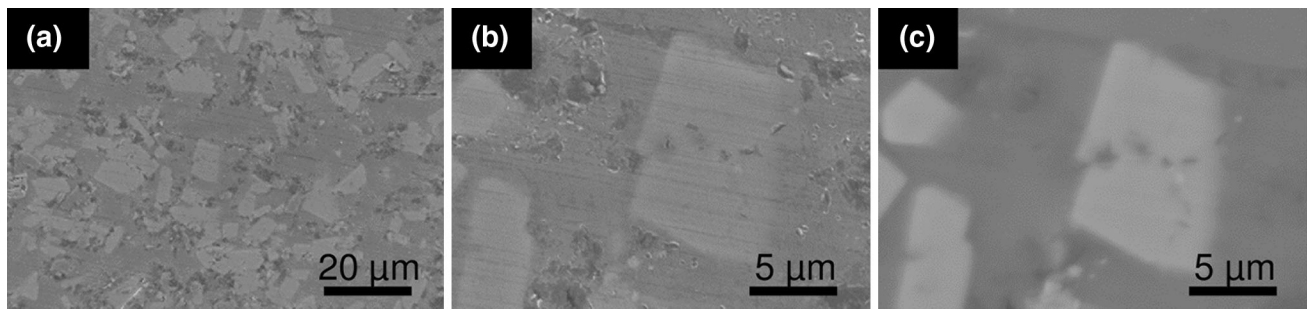


Fig. 3 SEM SE images of Al(80)-Ti₃SiC₂(20) composites at, (a) low, and (b) higher magnification and (c) BSE image of the higher magnification region

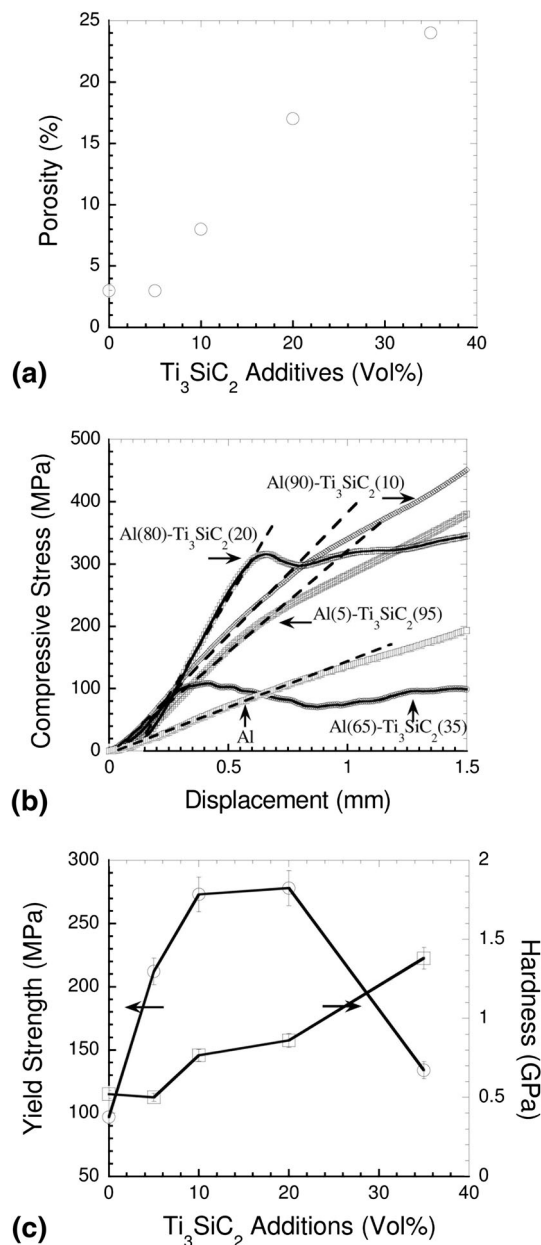


Fig. 4 Plot of, (a) porosity vs. vol.% of Ti₃SiC₂ additions in the Al matrix, (b) compressive stress vs. displacement profiles, and (c) yield strength (Y1 axis) and hardness (Y2 axis) vs. vol.% of Ti₃SiC₂ additions in the Al matrix

These results show that the addition of Ti₃SiC₂ particles remarkably improves the yield strength and hardness of the Al-matrix composites. Clearly, the presence of Ti₃SiC₂ particles reinforced the Al matrix. The lower yield strength of Al(65)-Ti₃SiC₂(35) samples can be attributed to the higher porosity of these composites (Fig. 4a).

3.3 Tribological Behavior

The tribological behavior of these composites was further investigated. Figure 5 shows the friction coefficient (μ) versus distance profile of all the composites. In general, during testing, μ showed a lot of fluctuations, however, the situation ameliorated as the content of Ti₃SiC₂ was increased in the Al matrix (Fig. 5e). For comparison, Fig. 6(a) plots the μ_f of all the composites. At a lower stress of ~ 0.12 MPa, the μ_f of Al was ~ 0.93 , whereas the μ_f of Al(95)-Ti₃SiC₂(5), Al(90)-Ti₃SiC₂(10), and Al(80)-Ti₃SiC₂(20) samples were ~ 0.76 , ~ 0.74 , and ~ 0.70 , respectively. Comparatively, μ_f of Al(65)-Ti₃SiC₂(35) was ~ 0.54 , and was significantly lower than all the other tested samples. At higher stresses, however, μ_f of Al decreased to ~ 0.68 and the μ_f of Al(95)-Ti₃SiC₂(5), Al(90)-Ti₃SiC₂(10), and Al(80)-Ti₃SiC₂(20) samples were similar to Al, but the μ_f of Al(65)-Ti₃SiC₂(35) was ~ 0.50 , and significantly lower. Thus, at higher concentration, Ti₃SiC₂ particulates have lubricating effect on the Al-matrix composites.

Figure 6(b) plots the WRs of all the composites. The WRs of all the compositions varied between $(2-6) \times 10^{-4}$ mm³/N m. The applied stresses did not have any significant effect on the WR on any composition, except Al, where the WR decreased marginally from 5.5×10^{-4} to 2×10^{-4} mm³/N m as the normal stress was increased from ~ 0.12 to ~ 0.62 MPa. More importantly, Ti₃SiC₂ particulates can decrease μ during sliding without having any adverse effect on the WRs.

3.4 Investigation of Tribosurfaces

Figure 7 shows the tribosurfaces of Al(80)-Ti₃SiC₂(20) and alumina. The Al(80)-Ti₃SiC₂(20) surface is covered with scuffing marks (Fig. 7a), and powdered and smeared third body debris was observed on both the surfaces (Fig. 7b, c). The EDS analysis of the Al(80)-Ti₃SiC₂(20) surface showed microconstituents with *Ti_{0.18}Si_{0.04}Al_{0.5}O_{0.24}{C_x}* (light color) and *Al_{0.34}Si_{0.01}Ti_{0.03}O_{0.63}{C_x}* (dark color) compositions, respectively. The EDS analysis indicates that there is intermixing and tribo-oxidation of different constituents during the tribology testing.

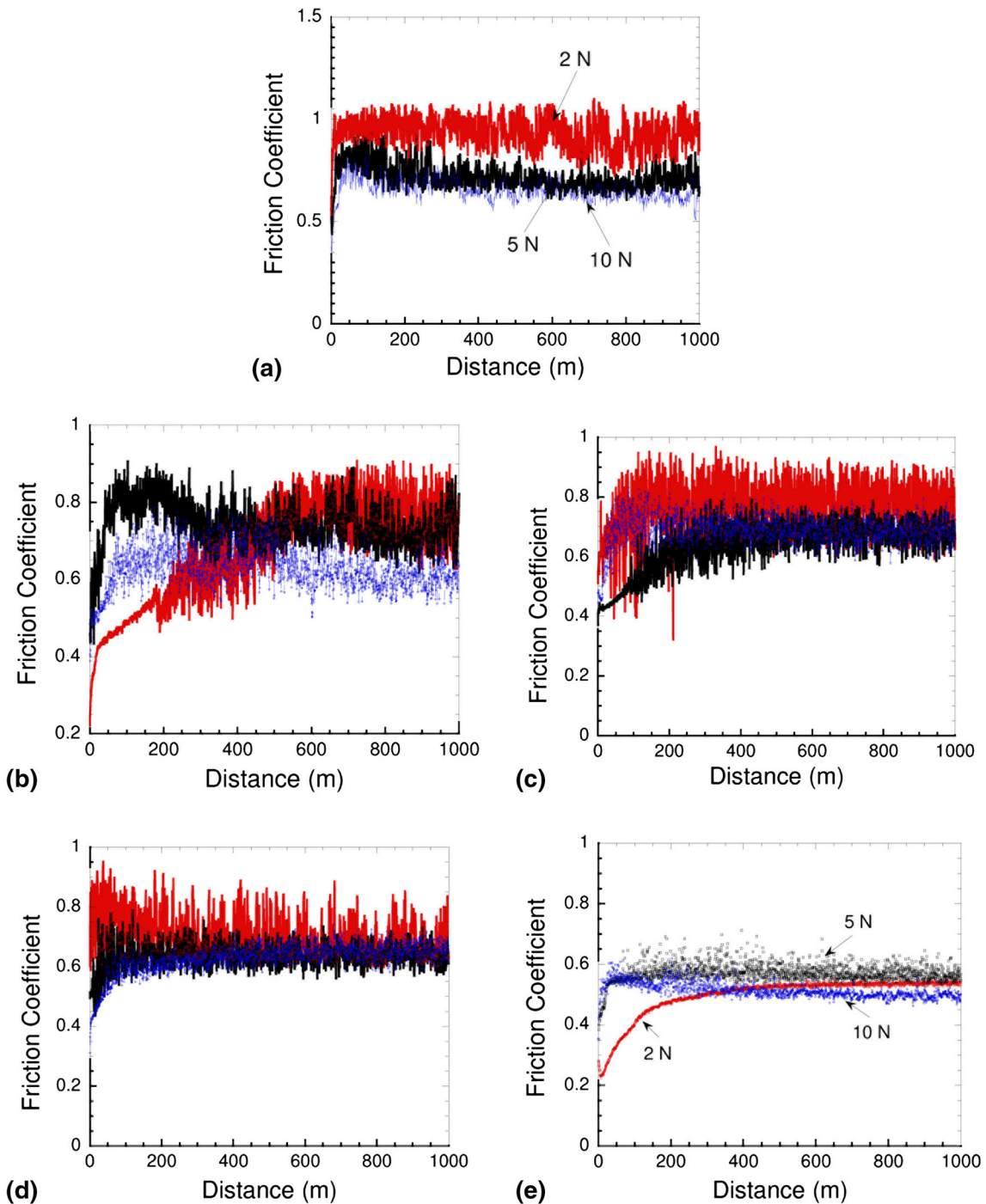


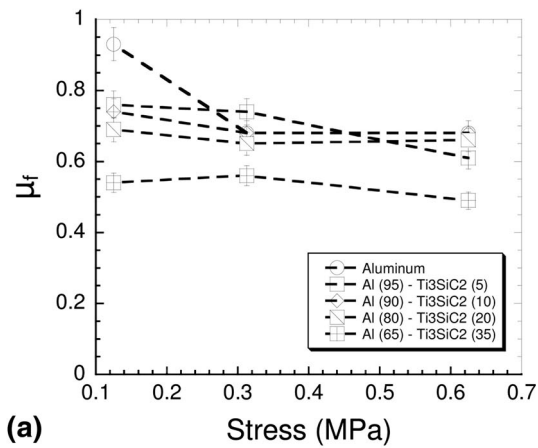
Fig. 5 Friction Coefficient (μ) vs. distance profile of, (a) Al, (b) Al(95)-Ti₃SiC₂(5), (c) Al(90)-Ti₃SiC₂(10), (d) Al(80)-Ti₃SiC₂(20), and (e) Al(65)-Ti₃SiC₂(35) against alumina substrates at different loads and 50 cm/s rotation speed. The red, black, and blue data points represent 2, 5, and 10 N, respectively

3.5 Mechanisms

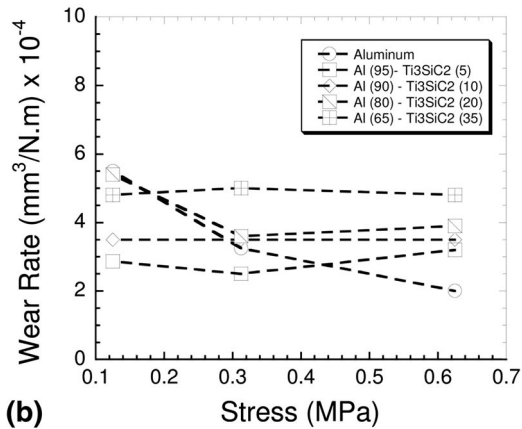
Recently, Gupta et al. (Ref 14) proposed a novel method of classifying tribofilms. A tribofilm can be classified into Type I if triboreactions occur predominantly at MAX surface; Types II if triboreactions occur at the tribopartner's surface; Types III if both MAX phase or their composites and the tribopartner contributes to the formation of tribofilms; and Type IV if MAX phase-based composites contribute predominantly to the triboreactions. Subsequently, Gupta et al. (Ref 14) had divided

these categories into sub-categories by taking into account the architectures and physical appearance of the tribofilms according to optical and SEM observations. The architectures of the tribofilms were mainly dependent on their degree of oxidation and mechanical integrity like adhesion to the substrate and hardness.

As discussed earlier, only Al-matrix surface is contributing the tribofilms formation, thus the tribofilms formed on the alumina surface can be categorized as Type IV. Gupta et al.



(a)



(b)

Fig. 6 Plot of, (a) final friction coefficient (μ_f) and (b) Specific Wear Rate (WR) vs. different applied stresses during dry sliding of Al-Ti₃SiC₂ composites against alumina

(Ref 14) had further classified the Type IV tribofilms as Type IVa and Type IVb. Type IVa tribofilms are lubricious and chemically homogenous at the microscale. It is because of the formation of phases, that the WRs ($\sim 10^{-5}$ mm³/N m) and μ 's (~ 0.4) were low in MAX/Ag composites. Type IVb tribofilms are composed of decomposed Ag-rich regions dispersed with different trioxides. At $\sim 6 \times 10^{-4}$ mm³/N m the WRs are high, but the μ 's (~ 0.4) were low.

The tribofilms observed during this study are patchy and powdery, thus they cannot be fitted into either of the above mentioned categories. The authors propose to classify these tribofilms as type IVc tribofilm. Morphologically, type IVc tribofilms is similar to type Ib tribofilms (Ref 14). Further optimization studies are needed to investigate whether the formation of powdery third bodies can be minimized in Al-Ti₃SiC₂ composite systems.

4. Conclusions

The authors report for the first time the synthesis and fabrication of Ti₃SiC₂ reinforced Al-matrix composites by pressureless sintering. The addition of Ti₃SiC₂ enhanced the mechanical and tribological performance of the Al-matrix composites. All the compositions, except Al(65)-Ti₃SiC₂(35), showed gradual failure. The Al(65)-Ti₃SiC₂(35) composition

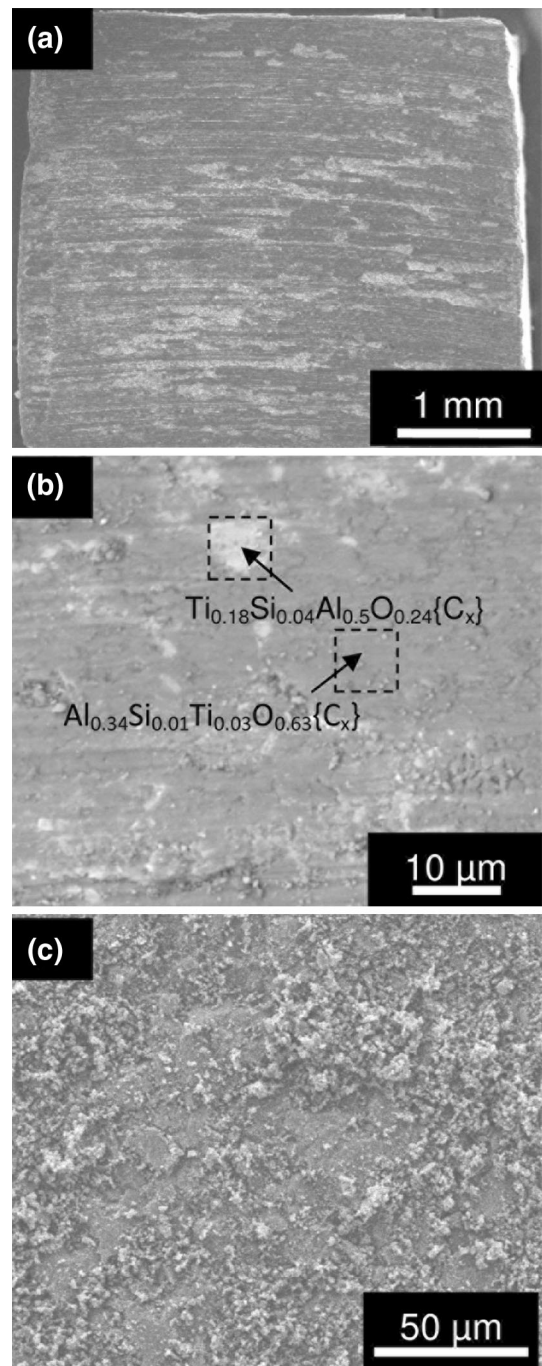


Fig. 7 SE SEM micrographs of the Ti₃SiC₂ surface at, (a) low, and (b) high magnification, and (c) alumina surface during dry sliding of Al (80)-Ti₃SiC₂(20) against alumina at 50 cm/s and 5 N at RT (room temperature)

showed brittle failure. The Al had a compressive strength of 97 ± 6 MPa, where as the volume fraction of Al was increased to 5 and 10 vol.% Ti₃SiC₂ in the composites, the compressive strength increased significantly to 212 ± 27 , and 273 ± 52 MPa, respectively. As the volume fraction of Ti₃SiC₂ was further increased to 20 vol.%, the compressive strength mildly increased to 278 ± 48 MPa. However, in Al(65)-Ti₃SiC₂(35), the compressive strength decreased to 134 ± 20 MPa. The hardness of the samples increased linearly as a function of Ti₃SiC₂ content. These results conclusively show

that the addition of Ti_3SiC_2 particles improves the mechanical behavior of the Al-matrix composites. The tribological behavior of the Al-matrix composites was also improved. The tribofilms observed between the interfaces was found to be powdery and patchy. The authors have classified these tribofilms as Type IVc. Nevertheless, more studies are needed to optimize the tribological behavior of these solids.

Acknowledgments

One of the authors (SG) would like to acknowledge the University of North Dakota start-up and seed grant funding for support. Authors would like to thank Kanthal Inc. for supplying the Ti_3SiC_2 powders. The XRD study in this work was supported in part by the MRSEC Program of the National Science Foundation under Award Number DMR-0819885. NDSU Electron Microscopy Center core facility is also acknowledged for the microscopy. This material is also based upon work supported by the National Science Foundation under Grant No. 0619098, and 1229417. Any opinions, findings, and conclusions or recommendations expressed in this material are those of the author(s) and do not necessarily reflect the views of the National Science Foundation.

References

1. M.W. Barsoum and M. Radovic, Elastic and Mechanical Properties of the MAX Phases, *Annu. Rev. Mater. Res.*, 2011, **41**, p 195–227
2. M.W. Barsoum and T. El-Raghy, Synthesis and Characterization of a Remarkable Ceramic: Ti_3SiC_2 , *J. Am. Ceram. Soc.*, 1996, **79**, p 1953–1956
3. M.W. Barsoum, The $M_{n+1}AX_n$ Phases: A New Class of Solids; Thermodynamically Stable Nanolaminates, *Prog. Solid State Chem.*, 2000, **28**, p 201–281
4. S. Amini, M.W. Barsoum, and T. El-Raghy, Synthesis and Mechanical Properties of Fully Dense Ti_2SC , *J. Am. Ceram. Soc.*, 2007, **90**(12), p 3953–3958
5. M. Radovic, M.W. Barsoum, T. El-Raghy, S.M. Wiederhorn, and W.E. Luecke, Effect of Temperature, Strain Rate and Grain Size on the Mechanical Response of Ti_3SiC_2 in Tension, *Acta Mater.*, 2002, **50**, p 1297–1306
6. T. El-Raghy, M.W. Barsoum, A. Zavalangos, and S.R. Kalidindi, Processing and Mechanical Properties of Ti_3SiC_2 . II. Effect of Grain Size and Deformation Temperature, *J. Am. Ceram. Soc.*, 1999, **82**, p 2855–2860
7. T. Zhen, M.W. Barsoum, S.R. Kalidindi, M. Radovic, Z.M. Sun, and T. El-Raghy, Compressive Creep of Fine and Coarse-Grained Ti_3SiC_2 in Air in the 1100–1300 °C Temperature Range, *Acta Mater.*, 2005, **53**, p 4963–4973
8. S.B. Li, L.F. Cheng, and L.T. Zhang, Oxidation Behavior of Ti_3SiC_2 at High Temperature in Air, *Mater. Sci. Eng. Struct. Mater. Prop. Microstruct. Process.*, 2003, **341**, p 112–120
9. S. Gupta and M.W. Barsoum, Synthesis and Oxidation of V2AlC and ($Ti_0.5, V_0.5$)2AlC in Air, *J. Electrochem. Soc.*, 2004, **151**, p D24–D29
10. M.W. Barsoum, N. Tzenov, A. Procopio, T. El-Raghy, and M. Ali, Oxidation of $Ti_{n+1}AlX_n$ ($n = 1–3$ and $X = C, N$). II. Experimental Results, *J. Electrochem. Soc.*, 2001, **148**, p C551–C562
11. X.H. Wang and Y.C. Zhou, Oxidation Behavior of Ti_3AlC_2 Powders in Flowing Air, *J. Mater. Chem.*, 2002, **12**(9), p 2781–2785
12. S. Gupta, D. Filimonov, and M.W. Barsoum, Isothermal Oxidation of Ta_2AlC in Air, *J. Am. Ceram. Soc.*, 2006, **89**, p 2974–2976
13. Z.J. Lin, M.S. Li, J.Y. Wang, and Y.C. Zhou, High-Temperature Oxidation and Hot Corrosion of Cr_2AlC , *Acta Mater.*, 2007, **55**, p 6182–6191
14. S. Gupta and M.W. Barsoum, On the Tribology of the MAX Phases and Their Composites During Dry Sliding: A Review, *Wear*, 2011, **271**, p 1878–1894
15. Y. Zhang, Z.M. Sun, and Y.C. Zhou, Cu/ Ti_3SiC_2 Composite: A New Electrofriction Material, *Mater. Res. Innov.*, 1999, **3**, p 80–84
16. S. Gupta, D. Filimonov, T. Palanisamy, T. El-Raghy, and M.W. Barsoum, Ta_2AlC and Cr_2AlC Ag-Based Composites: New Solid Lubricant Materials for Use Over a Wide Temperature Range Against Ni-Based Superalloys and Alumina, *Wear*, 2007, **262**, p 1479–1489
17. B. Anasori, S. Amini, V. Presser, and M.W. Barsoum, *Nanocrystalline M-Matrix Composites with Ultrahigh Damping Properties*. Magnesium Technology, Wiley, Hoboken, 2011, p 463–468
18. W.J. Wang, V. Gauthier-Brunet, G.P. Bei, G. Laplanche, J. Bonneville, A. Joulain, and S. Dubois, Powder Metallurgy Processing and Compressive Properties of Ti_3AlC_2/Al Composites, *Mater. Sci. Eng. A*, 2011, **530**, p 168–173
19. L. Hu, A. Kothalkar, M. O'Neil, I. Karaman, and M. Radovic, Current-Activated, Pressure-Assisted Infiltration: A Novel, Versatile Route for Producing Interpenetrating Ceramic-Metal Composites, *Mater. Res. Lett.*, 2014, doi:[10.1080/21663831.2013.873498](https://doi.org/10.1080/21663831.2013.873498)
20. A. Kothalkar, R. Benitez, L. Hu, M. Radovic, and I. Karaman, Thermo-mechanical Response and Damping Behavior of Shape Memory Alloy/MAX Phase Composites, *Metall. Mater. Trans. A.*, 2014, **45**, p 2646–2658
21. K.G. Budinski and M.K. Budinski, *Engineering Materials Properties and Selection*, 9th ed., Prentice Hall, Upper Saddle River, 2010
22. D.B. Miracle, Metal Matrix Composites: From Science to Technological Significance, *Compos. Sci. Technol.*, 2005, **65**, p 2526–2540
23. Z. Chen, T. Takeda, and K. Ikeda, Microstructural Evolution of Reactive-Sintered Aluminum Matrix Composites, *Compos. Sci. Technol.*, 2008, **68**, p 2245–2253
24. A. Pramanik, L.C. Zhang, and J.A. Arsecularatne, Machining of Metal Matrix Composites: Effect of Ceramic Particles on Residual Stress, Surface Roughness and Chip Formation, *Int. J. Mach. Tools Manuf.*, 2008, **48**, p 1613–1625
25. M. El-Gallab and M. Sklad, Machining of Al/SiC Particulate Metal-Matrix Composites, Part I: Tool Performance, *J. Mater. Process. Technol.*, 1998, **83**, p 151–158
26. X. Ding, W.Y.H. Liew, and X.D. Liu, Evaluation of Machining Performance of MMC with PCBN and PCD Tools, *Wear*, 2005, **259**, p 1225–1234